Membrane lipids are key-modulators of the endocannabinoid-hydrolase FAAH

Enrico Dainese[1,2¥*], Gianni De Fabritiis[3¥], Annalaura Sabatucci[1], Sergio Oddi[1,2], Clotilde Beatrice Angelucci[1], Chiara Di Pancrazio[1], Toni Giorgino[4], Nathaniel Stanley[3], Michele Del Carlo[5], Benjamin Cravatt[6] and Mauro Maccarrone[2,7*]

[1]Department of Biomedical Sciences, University of Teramo, Teramo, Italy, [2]European Center for Brain Research (CERC)/Santa Lucia Foundation, Rome, Italy, [3]Computational biochemistry and biophysics laboratory, (GRIB-IMIM), University of Pompeu Fabra, Barcelona Biomedical Research Park (PRBB), Barcelona, Spain, [4] Institute of Biomedical Engineering, National Research Council of Italy (ISIB-CNR), Padua, Italy, [5]Department of Food Science, University of Teramo, Teramo, Italy, [6]Departments of Cell Biology and Chemistry, The Skaggs Institute for Chemical Biology, The Scripps Research Institute, La Jolla, California, [7]Center of Integrated Research, Campus Bio-Medico University of Rome, Rome, Italy.

Short title: FAAH is modulated by membrane cholesterol.

¥*Equally first authors*.
**Corresponding authors*: e-mail: edainese@unite.it, tel. and Fax +39 0861 266876; m.maccarrone@unicampus.it, tel. and Fax: +39 06 2254 19169.

Abbreviations used: SAXS, small angle X-ray scattering; FAAH, fatty acid amide hydrolase; AEA, anandamide (*N*-arachidonoylethanolamine); HPLC: high pressure liquid chromatography; SDS: sodium dodecyl sulphate; MAFP: methoxyarachidonoyl fluorophosphonate; DPPC: 1,2-dipalmitoyl-*sn*-glycero-3-phosphocholine; POPC: 1-palmitoyl-2-oleyl-*sn*-glycero-3-phosphocholine; Py-PE, 1,2-dioleoyl-*sn*-glycero-3-phosphoethanolamine-*N*-1-pyrenesulfonyl; FRET: fluorescence resonance energy transfer; LUVs, large unilamellar vesicles.

Abstract

Lipid composition is expected to play an important role in modulating membrane enzyme activity, in particular if the substrates are themselves lipid molecules. A paradigmatic case is fatty acid amide hydrolase (FAAH) a critical enzyme in terminating the endocannabinoid signalling and an important therapeutic target. Here, using a combined experimental and computational approach, we show that membrane lipids modulate structure, subcellular localization and activity of FAAH. We report that FAAH dimer is stabilized by the lipid bilayer and shows higher membrane binding affinity and enzymatic activity within membranes containing both cholesterol and the natural FAAH substrate, anandamide (AEA). Additionally, colocalization of cholesterol, AEA, and FAAH in mouse neuroblastoma cells suggests a mechanism through which cholesterol increases the substrate accessibility of FAAH.

Keywords: cholesterol/endocannabinoids/FAAH/membrane

Summary statement

The dimeric structure of FAAH is stabilized by the membrane.
Membrane binding affinity of FAAH is relevant for subcellular localization.
Free cholesterol within the membrane increases the activity of the enzyme.
Molecular dynamic studies suggest that cholesterol increases substrate accessibility.

INTRODUCTION

Fatty acid amide hydrolase (FAAH) is a membrane-bound enzyme that is responsible for the intracellular hydrolysis of the bioactive lipid anandamide (*N*-arachidonoylethanolamine, AEA) and other congeners known as endocannabinoids (eCBs) [1]. The discovery of FAAH [2], and the demonstration that it terminates the signalling and biological activity of AEA *in vivo*, has inspired pharmacological strategies aimed at augmenting the eCB tone through FAAH inhibitors (see for review [3]). The three-dimensional structure of FAAH has been resolved at high resolution for a truncated form of the rat enzyme [4], and for a humanized form of the same enzyme where specific residues were substituted to generate a human-like active site [5]. The collected structural information allowed to disclose the catalytic mechanism of FAAH, but a role for the surrounding membrane lipids in controlling enzyme activity remains as yet unknown.

Membrane lipid composition affects eCB uptake and signalling, and accumulated evidence demonstrates that cholesterol is a key determinant of this regulation [6]. In many cell-types cholesterol removal by methyl-β-cyclodextrins dose-dependently reduced the uptake of AEA [6], that instead was increased by cholesterol enrichment [7]. A contributing factor to this effect may be the affinity of cholesterol towards AEA [8]. In the same context, cholesterol has been shown to modulate AEA binding to type-1 (CB_1) cannabinoid receptor [9], and type-1 vanilloid (TRPV1) receptor [10]. It has been proposed very recently a role for cholesterol in the modulation of AEA transport across the membrane, leading to a consequent increase of AEA hydrolysis by FAAH [11]. However, a description of the possible molecular mechanism of direct FAAH modulation by cholesterol is still missing. In C6 glioma cells either cholesterol enrichment or depletion in the plasma membrane did not modulate FAAH activity [6], but due to a fine regulation of cholesterol homeostasis within the cell, a variation of membrane cholesterol content is unlikely to promptly influence cholesterol concentration within the intracellular compartments (see for review [12]).

With the aim of dissecting the requirements for the catalytic activity and those for the enzyme interaction with membranes, we analysed by small angle X-ray scattering (SAXS) and fluorescence resonance energy transfer (FRET) the conformational changes induced by lipid bilayers on FAAH. Both using synthetic or reconstructed lipid vesicles from different cell compartments (i.e., plasma membrane (PM) or endoplasmic reticulum (ER)), we demonstrated a key-role of membrane lipids in stabilizing a dimeric form of FAAH with cholesterol and AEA, that both modulate its enzymatic activity within the membrane. Furthermore, molecular dynamics simulations supported a novel mechanism by which cholesterol may help to open the membrane port of FAAH [4], thus increasing the accessibility to the enzyme substrate, AEA. Overall, these results further our understanding of the molecular events underpinning the modulation of membrane enzymes by the surrounding lipids. FAAH has been proposed as a paradigm of such membrane enzymes that bind lipophilic substrates (generally embedded within the membrane) and cleave them with water to release hydrophilic products [13].

EXPERIMENTAL

Reagents and antibodies

All chemicals were of the purest analytical grade. *N*-Arachidonoylethanolamine (anandamide, AEA), cholesterol, arachidonic acid (AA), ethanolamine, *N*-palmitoylethanolamine, *N*-stearoylethanolamine, dipalmitoylphosphatidylcholine (DPPC) and the Protease Inhibitor Cocktail were from Sigma Chemical Co. (St. Luis, MO, USA). 1-Palmitoyl-2-oleyl-*sn*-glycero-3-phosphocholine (POPC), dioleoylphosphatidylcholine (DOPC), brain sphingomyelin (containing almost exclusively C18:0), and cholesterol were purchased from Avanti Polar Lipids (Alabaster, AL, USA). Isopropyl-β-D-thiogalactopyranoside (IPTG) was purchased from Promega Corporation (Madison, WI, USA), threalose was from Cargill Inc. (Davison, MI, USA), and the Talon resin was from Clontech (Mountain View, CA, USA). Biotin-AEA (b-AEA) was synthesized as reported [14].

Cy2-streptavidin and DyLight 405-streptavidin were purchased from Jackson ImmunoResearch Labs (West Grove, PA, USA). Alexa Fluor 555-conjugated cholera toxin subunit B, donkey anti-rabbit Alexa Fluor-conjugates secondary antibodies and Prolong Gold anti-fade kit were purchased from Invitrogen (Milan, Italy). Rabbit anti-FAAH polyclonal antibody was purchased from Primm (Milan, Italy).

Small angle X-ray scattering measurements

SAXS measurements were performed using the SWING beamline at the SOLEIL synchrotron radiation facility (Saint-Aubin, France). The measuring cell under vacuum was kept at constant temperature (10°C) during measurements. Twenty-five frames of 1s each were recorded and averaged after visual inspection for radiation damage (none was found). The scattering intensities were measured over the q-range q_{min}=0.0005 Å^{-1} q_{max}=0.50 Å^{-1} ($q=(4\pi/\lambda)\sin\theta$, 2θ being the scattering angle). FAAH samples were measured at a concentration of ~1.0 mg/ml. The radius of gyration (Rg) and the molecular mass of the proteins were calculated through the Guinier approximation [15]. The distance distribution function p(r) was determined using the indirect Fourier transform method, as implemented in the GNOM program package [16]. *Ab initio* calculations of the FAAH shape from the SAXS pattern were performed using the DAMMIN program [17]. Ten independent calculations were performed, averaged and filtered after their consistency with the SUPCOMB program [18], as already described [19]. All obtained models yielded very similar shapes, as shown by the low value (0.651±0.012) of the normalized spatial discrepancy (NSD), calculated with the DAMAVER program suite [20]. Being FAAH a membrane enzyme prone to aggregation in aqueous solutions, we evaluated the best experimental conditions able to stabilize soluble forms of the protein, suitable for SAXS analysis. We found that, among several factors, concentrations of Tris/HCl buffer ≥ 0.5 M, and high ionic strength with salt (e.g. NaCl) concentrations ≥ 0.1 M, are able to avoid the formation of insoluble aggregates. Thus, the purification and the stabilization of the protein was carried out with 0.1 M NaCl dissolved in 0.5 M Tris/HCl buffer, pH 7.5. SAXS data under these experimental conditions were used to obtain the overall conformation of FAAH in solution.

The possible effect of different membrane lipid compositions on FAAH structure was also investigated by SAXS using 1-palmitoyl-2-oleyl-*sn*-glycero-3-phosphocholine (POPC), 1,2-dipalmitoyl-*sn*-glycero-3-phosphocholine (DPPC) and the major FAAH substrate, AEA, at a sub-micellar concentration (<20μM) [21]. None of these experimental conditions affected the scattering curve of FAAH oligomers. Higher lipid concentrations were not used, because they form micellar structures with a volume several times larger than that of FAAH, thus completely masking the scattering signal of the protein.

Membrane binding measurements

Fluorescence spectra were recorded at 25°C using a Perkin Elmer LSB50 fluorimeter (PerkinElmer Life and Analytical Sciences, Boston, MA, USA) and 10x2 mm pathlength quartz fluorescence

microcuvettes (Hellma, Plainview, NY, USA). Pyrene-liposomes used in fluorescence resonance energy transfer (FRET) studies contained 5% (w/w) 1,2-dioleoyl-*sn*-glycero-3-phosphoethanolamine-*N*-1-pyrenesulfonyl (Py-PE), that was purchased from Molecular Probes (Eugene, OR, USA). FAAH was used at a final concentration of 0.2 μM, while liposome concentration varied between 10 and 600 μM in a final volume of 100 μl. Solutions containing freshly prepared FAAH and Py-PE liposomes were used in all experiments. Emission spectra (λ_{ex} = 292 nm, and λ_{em} = 300-420 nm) were recorded in lysis buffer without trehalose. Data were plotted as fractional loss of Trp fluorescence ($\Delta F/\Delta F_{max}$) *versus* liposome concentration, as previously described [22]. Experimental data were analyzed by nonlinear regression through an hyperbolic binding isotherm, using the Kaleidagraph program (Synergy Software, Reading, PA, USA). Large unilamellar vesicles (LUVs) were prepared with POPC, as previously described [22]. LUVs containing lipid rafts (indicated as lipid rafts) were prepared with DOPC, brain sphingomyelin, and cholesterol in an equimolar ratio (1:1:1), as reported [23]. Cholesterol- and AEA-enriched LUVs were prepared using POPC, AEA, and cholesterol at molar ratios from 10:1:1 to 10:1:5. The same vesicles were prepared also with PEA, SEA, AA, and ethanolamine instead of (and at the same molar ratio as) AEA.

Cell membranes isolation and characterization

PM and RE membranes were isolated from rat liver as previously reported [24] with some modifications. Briefly, the hepatic tissue was disrupted using a Potter glass, and mixed with an equal volume of disruption buffer (5 mM Tris/HCl pH 7.8, containing 10 mM KCl and 5 mM EDTA, HB). After centrifugation at 2,000 *g* for 5 min the supernatant was transferred to a 12 mL ultracentrifugation tube, and was sequentially overlaid with 9.6 mL of 60 % sucrose buffer, 4.5 ml of 37 % sucrose buffer, and Top solution (1 ml of HB) followed by centrifugation at 150 000 *g* for 2 h. In the last step the PM and the membrane of the ER was recovered with a glass Pasteur pipette, washed with the HB buffer and then centrifuged for 1 h at 150,000 *g*. The final pellet was dried for 12 h in an essicator and stored at -20°C until use. The analysis of phosphatidylethanolamine (PE), phosphatidylserine (PS), phosphatidylcloline (PC) and sphingomyelin (SM) in PM and ER extracted from liver was carried out by HPLC in a Luna Silica Column 3mm, 150x4.6 mm (Phenomenex Inc., Torrance, CA, USA), using acetonitrile-methanol-85% phosphoric acid (100:10:0.8, V/V) as mobile phase (flow rate 1ml/min) and an UV detector set at 205 nm (Perkin Elmer Inc., Waltham, MA, USA). Quantitative analysis was performed by the external standard method for each of the investigated lipids; the calibration linear range was 0.010–2.000 mg/ml. PM and ER extracts were dissolved in chloroform and injected in the HPLC system without further treatment. Identification of the compound was based on retention time. Cholesterol quantification was obtained with the same chromatographic column using hexane-isopropanol (99:1, V/V) as mobile phase (flow rate 0.6 ml/min) and an UV detector set at 202 nm. The calibration linear range was 0.005–1.500 mg/ml, sample extracts were dissolved in chloroform and injected in the HPLC system.

Imaging and co-localization analysis

All experiments were carried out on a Leica TCS SP5 DMI6000 confocal microscope (Leica Microsystems, Wetzlar, Germany). Details of cell culture, treatment and staining are reported in the Supplementary Methods. For co-localization analysis, we determined the Pearson's correlation coefficient and the intensity correlation quotient, by using the ImageJ plugin JACoP that groups together the most important co-localization tools [25]. Values for Pearson's correlation coefficient can range from +1 to -1: +1 represents a perfect correlation, -1 represents a perfect exclusion, and 0 represents a random localization [26]. In addition, apparent co-localization due to random staining, or very high intensity, in one window will have values of intensity correlation quotient near to zero, while if the two signal intensities are interdependent (co-localized) these values will be positive with a maximum of 0.5 [27].

Statistical analysis

Data reported in this paper are the mean (± S.D.) of at least four independent determinations, each performed in triplicate. Statistical analysis was performed by the non-parametric Mann-Whitney U test, analyzing experimental data by means of the Prism 5 program (GraphPAD Software for Science, San Diego, CA, USA).

Molecular dynamics simulations

All molecular dynamics simulations were performed using ACEMD [28] locally and on the GPUGRID.net distributed computing network [29]. All simulations were all-atom, explicit solvent simulations using TIP3P water. The CHARMM 27 force field [30] was used for the protein; CHARMM Lipid C36 parameters [31] were used for POPC and cholesterol, and CHARMM-GUI [32] was used to build membrane components. The protein structure was taken from Protein Data Bank (PDB) ID 1MT5, but with the MAFP inhibitor removed. AEA was parameterized using CGenFF forcefield through the ParamChem web service [33]. Details about setup, equilibration, and production runs of all simulations are reported in the Supplementary information.

RESULTS

FAAH structure is modulated by membranes

The truncated form of rat FAAH resolved at 2.8 Å by x-ray crystallography [4] was used in this investigation, and its conformation in solution was analyzed by SAXS. As calculated from the p(r) function (and in accordance with the Guinier analysis) (Fig. 1A,B), SAXS data of FAAH yielded a radius of gyration of 129±13 Å, and a value of the maximum dimension of the particle (D_{max}) of 410±10 Å. *Ab initio* calculations of the shape of the molecule, performed from the SAXS pattern with the DAMMIN program [17], indicated that FAAH has an overall structure with three lobes. Each of them is well-fitted by the crystallographic unit of the protein, that is an octamer of dimers (Supplementary Scheme 1). Indeed, superimposing the crystallographic unit of FAAH (pdb entry 1MT5.pdb) on the low resolution DAM models of the oligomers, it appears that in the absence of detergents FAAH is composed of three octamers (Fig. 1C). Thus, the enzyme shows a peculiar topology in solution, where the crystallographic unit seems to behave as a building block for an oligomeric structure elongating along a specific axis, thus leading to an unprecedented structural organization of the enzyme (Fig. 1C). In order to mimic the membrane milieu, we used detergents with a small micellar volume [34]. In the presence of 1% (W/V) Triton X-100 we obtained a scattering profile where a typical oscillation corresponding to the micellar structure of the detergent was evident (Fig. 2, arrow).

The Guinier analysis of this scattering curve yielded a value of the radius of gyration of 35.6±0.2 Å (Fig. 2), very similar to the theoretical value obtained from the dimeric biological unit of the crystallographic structure [4] (Supplementary Scheme 1). Thus, in the presence of the detergent FAAH is mainly organized as a dimer, suggesting that upon interaction with membranes the oligomeric form of FAAH dissociates. Interestingly, Triton X-100 did not affect the dependence of FAAH activity on substrate concentration, that followed a typical Michaelis-Menten kinetics yielding K_m, k_{cat} and k_{cat}/K_m values of 16 ± 3 μM, 5.6 ± 0.6 s^{-1}, and 3.5×10^5, respectively, in the presence and in the absence of the detergent. Incidentally, these values are in line with those already reported for FAAH by others [2;35]. Since the dissociated FAAH dimers had the same kinetic properties as the oligomeric form of the enzyme (not shown), it can be concluded that aggregation does not influence enzyme activity.

To further understand the effect of membranes on FAAH structure and function, we analyzed the intrinsic fluorescence of the enzyme in the presence of large unilamellar vesicles (LUVs) constituted by POPC. The fluorescence spectrum of FAAH is very broad, due to the presence of more than one emitting species [36]; yet, increasing the concentration of POPC vesicles led to a relevant red-shift of

the wavelength at the emission maximum (λ_{max} from 343.5 to 346.0 nm) (Supplementary Fig. 1). Interestingly, this effect was not replicated by simply diluting the enzyme, which suggests an overall higher exposure of the aromatic residues of the protein to the water solvent in the presence of membranes (Supplementary Fig. 1). Instead, the observed red-shift seems to be attributable to a general increase in the solvation of the protein, due to the dissociation of the octameric structure.

FAAH preferentially binds to membranes containing both AEA and cholesterol

The structural analysis was further extended by measuring the membrane binding properties of FAAH through fluorescence resonance energy transfer (FRET). To ascertain whether FAAH had any preference for specific membranes, we made LUVs of different lipid compositions. Membrane binding of FAAH was not affected by the physicochemical properties of the membrane, because half-saturation binding values ($[L]_{1/2}$) were similar with membranes in liquid disordered crystalline phase (POPC vesicles) and in solid-like gel phase (β-phase) (DPPC vesicles) (Table 1). Therefore, in subsequent FRET experiments only POPC LUVs were used. Remarkably, POPC is abundant in animal cell membranes [37]. A role for cholesterol in modulating AEA movement within the membrane has been recently reported in biophysical studies [8;38]. Here, we found that the co-presence of AEA and cholesterol within POPC membranes, at a stoichiometric ratio from 1:1 to 1:5, induced a pronounced decrease of $[L]_{1/2}$ (14.7 ± 3.0); this indicates a strong increase (~5-fold over the POPC control) of the affinity of FAAH for AEA/cholesterol-containing membranes (Table 1, and Supplementary Figure 2).

To ascertain whether this preferential interaction could be ascribed to a general modification of the physicochemical properties of the membrane, or was rather due to the presence of a specific class of polyunsaturated lipids or functional groups, we tested also the effect of AEA hydrolysis products (arachidonic acid (AA), and ethanolamine), and of other fatty acid amides, such as *N*-stearoylethanolamine and *N*-palmitoylethanolamine. In all cases higher $[L]_{1/2}$ values were obtained (Table 1), demonstrating that the preferential binding of FAAH occurred only with membranes containing AEA. As expected for a membrane enzyme associated with the ER [3], FAAH shows a higher binding affinity for membranes in the liquid disordered state (POPC) and a weaker interaction with lipid rafts structures typical of the PM [39]. Thus, we further tested whether the preferential binding of FAAH was maintained in lipid rafts-containing membranes.

Embedding AEA within lipid rafts-containing LUVs [23] did not significantly affect the binding of FAAH (Table 1, Supplementary Figure 2), overall suggesting that this enzyme prefers membranes containing AEA within cholesterol-rich regions in the liquid disordered phase, rather than organized in lipid rafts. We extended these experiments further by analysing FAAH binding to PM and ER membranes isolated from rat liver, as described in Supplementary methods. These results showed that FAAH preferentially binds to ER membranes (containing ~ 3% mol/mol of cholesterol) (Supplementary Table 1), yielding $[L]_{1/2}$ values very similar to those obtained with AEA/cholesterol-containing synthetic vesicles (Table 1, and Supplementary Figure 2). It should be recalled that ER membranes are the primary sites of accumulation of AEA (Supplementary Figure 3).

FAAH activity is modulated by cholesterol

To clarify whether the preferential interaction of FAAH with AEA/cholesterol-containing membranes could influence also the enzyme activity, we measured AEA hydrolysis by FAAH in the presence of different synthetic membranes. FAAH showed a similar catalytic activity in solution and when bound to POPC vesicles (Figure 3). Externally adding FAAH to POPC vesicles that contained increasing AEA/cholesterol molar ratios (from 1:1 to 1:5), an increased enzyme activity up to ~4-fold over the controls was observed (Fig. 3), indicating that FAAH activity can be modulated by the co-presence of cholesterol and AEA within the membrane in a cholesterol concentration-dependent

manner (Fig. 3). This effect can be explained by the increased affinity of FAAH for membranes containing both AEA and cholesterol (Table 1), leading to higher amounts of membrane-embedded enzyme with respect to the control. Incidentally, the cholesterol/POPC ratio did not affect the specific activity of FAAH.

FAAH colocalizes with AEA and cholesterol in mouse neuroblastoma cells

Fluorescence microscopy analysis of mouse N18 neuroblastoma cells revealed that FAAH is distributed in several dotted structures widely diffused in the cytoplasm, and particularly prominent in the perinuclear zone (Fig. 4). These findings extend previous studies showing that FAAH is primarily associated with membranes of the ER, and excluded from the PM [40]. To compare the degree of association of FAAH with different lipids and/or membrane compartments, a series of co-staining experiments was performed with specific lipid markers: biotinil-AEA (b-AEA), a stable analogue of AEA, was used to stain ER and adiposomes [41]; filipin, a fluorescent macrolide that specifically binds to both raft and non-raft membrane cholesterol, was used to stain free cholesterol [9]; Alexa Fluor 555-conjugated cholera toxin B (CTB) was used to stain ganglioside GM1, a lipid selectively confined to lipid rafts [9]. The extent of spatial overlap among FAAH and these lipids was measured using the Pearson's correlation coefficient, a widely accepted parameter to quantify the degree of colocalization between fluorophores [41]. A strong association between b-AEA and FAAH was found in N18 cells, with a higher colocalization between filipin-stained cholesterol and AEA, and a smaller (yet significant) association between filipin and FAAH (Fig. 4). In contrast, FAAH staining did not significantly overlap with that of CTB (Fig. 4), suggesting a lower affinity of FAAH for authentic lipid rafts. Overall, FAAH appears to be mainly localized in AEA and cholesterol containing regions of internal membranes, but not in plasma membrane lipid rafts.

Molecular dynamics simulation of FAAH within the membrane

The change in the catalytic activity of FAAH in the presence of cholesterol suggests a plausible entry pathway for AEA from the lipid bilayer. Indeed, a 200 ns long molecular dynamics (MD) simulation of FAAH embedded in the membrane showed that the protein relaxes to a pose similar to what already presented in the literature [4], with the accessible entry of the AEA binding pocket at the interface between the polar head of the membrane and the solvent. Such a pose is compatible with the entry pathway of AEA into the binding cavity from the membrane.

In order to better understand the effect of cholesterol on AEA binding to FAAH, we simulated the full event of binding of the substrate itself [42], thus ascertaining whether a direct interaction with cholesterol may explain the preferential membrane binding and the increased catalytic activity of FAAH. We performed more than 1,500 parallel simulations of FAAH associated with a membrane containing AEA:cholesterol:POPC at 1:5:10 molar ratio, each for an average of 165 ns, totalling over 250 μs of sampling time. Of these, 1,000 simulations were free ligand binding simulations [42], in which 26 binding events were seen. An additional 550 simulations resampled these 26 events in order to improve binding analysis and to clarify how AEA may explore the enzyme inside. The data yielded an interesting picture of AEA binding to FAAH (Fig. 5, and Supplementary Video 1), suggestive of a specific role for cholesterol in the modulation of the enzyme activity. AEA approached FAAH at the previously proposed membrane port [4], exploring the pocket formed by helices α17, α18, α19 and the loop between sheet β9 and helix α22 (Fig. 5C1). The primary barriers to entry were steric hindrance by side chains and a salt bridge formed between those secondary structure elements. Once these barriers were overcome, the polar head group of AEA moved into the enzyme, where it formed weak and transient hydrogen bonds with water and the backbone of helix α9 and helix α22, as well as with the loop preceding it (Fig. 5C2). AEA then displaced more water from the enzyme and moved further up

into the enzyme (Fig. 5C3), at which point the primary barrier was the highly disordered internal structure of the enzyme (in particular the very large loop between sheet β3 and helix α8), as well as further AEA dehydration. Finally, AEA took a similar pose to that shown for the MAFP inhibitor in the crystal structure (Fig. 5C4).

The most significant outcome of MD simulations was the possible explanation of the role of cholesterol in increasing AEA binding. When the salt bridge is intact, it closes the enzyme gate and AEA is prevented from entering. The continued interaction with the cholesterol head group helps to maintain the port open while AEA enters, and allows other side chains to take conformations that make AEA binding easier. Cholesterol remains close to the enzyme even after AEA has fully entered, continuing to interact with the residues that keep the port open and fitting snugly against the enzyme in the region where AEA was before entering. In membranes made of AEA:POPC only, the probability that another lipid (e.g., another AEA) donates a hydroxyl group for the same purpose would be significantly lower. Overall, MD simulations seem to explain the role of cholesterol in increasing FAAH activity, as measured experimentally (Fig. 4).

The exit of the AEA cleavage reaction products (i.e., ethanolamine and arachidonic acid) is unlikely to be strongly modulated by cholesterol, while a role could also be played by increased lateral diffusion of AEA in cholesterol-containing membrane domains. To address this point, diffusion coefficients were computed for AEA through MD simulations. For the AEA:POPC (9:75) and the AEA:Chol:POPC (9:45:75) systems these coefficients were found to be, respectively, 16.9 ± 5.9 and $13.6 \pm 5.0 \times 10^{-8}$ cm^2/s, with no statistically significant difference. Incidentally, these values of the diffusion coefficients are consistent with previous data obtained experimentally [43]. Next, we investigated whether the effect of cholesterol on FAAH activity could be related also to an increased interlayer (flip-flop) movement of AEA [8], measured as cholesterol-dependent increase in the AEA flip-flop rate between bilayers. Using all atom simulations (see Supplementary Information), we did observe a qualitative higher flip-flop rate for AEA with cholesterol.

DISCUSSION

The crystallographic unit of FAAH is constituted by octamers of dimers and the derived biological unit is a dimeric protein [4] (Supplementary Scheme 1). SAXS measurements reported here show that in solution FAAH adopts a higher hierarchical organization of its quaternary structure, constituted by three octamers of dimers (Fig. 1). Combined SAXS and fluorescence analyses show that the binding of FAAH to membranes (or to detergents that mimic the membrane milieu) induces a dissociation of these oligomers, and stabilizes the dimeric form of the enzyme. Remarkably, the dimer of FAAH is a functional unit with the same catalytic activity as the octamer.

Additional FRET measurements allowed to assess the preferential interaction of FAAH with membranes containing both AEA and cholesterol, yet not organized in lipid rafts. The ~5-fold increase of FAAH affinity for membranes in the presence of cholesterol and AEA appears to be specific for AEA and not for other eCBs, and is not observed with either lipid alone. Moreover, data obtained with PM and ER membranes from rat liver are superimposable on those obtained with synthetic vesicles. In particular, considering that ER membranes contain ~3% of cholesterol and that AEA is mainly localized in this compartment (Supplementary Fig. 3), our data strongly suggest a physiological role of these lipids in maintaining the proper intracellular localization of FAAH.

By confocal analysis we revealed that FAAH is consistently confined to AEA/cholesterol-rich regions, with very low association with GM_1-rich membrane domains on the cell surface (Fig. 4). Such a preferential binding of FAAH could contribute *in vivo* to maintain the enzyme stably localized in a compartment with more efficient hydrolysis of AEA within cell membranes containing non-raft cholesterol, such as those of ER, or those of intracellular stores of AEA like the adiposomes [24].

FAAH mainly interacts with one leaflet of the membrane bilayer (Fig. 5A), thus it is conceivable that AEA reaches the active site of the enzyme only from that leaflet *via* the so-called membrane port [4]. Cholesterol could induce a higher catalytic activity of FAAH by directly interacting with the enzyme, thus increasing the accessibility to AEA of the membrane port. Consistently, our MD studies clearly indicate that the binding of AEA is directly aided by cholesterol that is more concentrated around the membrane port of FAAH (Fig. 5B). Through its interaction with key salt bridge residues that gate AEA entrance, cholesterol facilitates port opening, so that AEA can enter and reach the active site of the enzyme.

These results support the concept of a substrate-enzyme interaction, whereby a third player comes into the game: the membrane lipids. In the case of metabolic enzymes of eCBs, these observations might have therapeutic relevance. On a more general note, this investigation sheds light on the key-role of the lipid environment in determining biological activity. This concept emerged in recent years for membrane receptors [44], and here we show that it holds true also for a membrane enzyme like FAAH, that is at the heart of eCB signalling in many pathophysiological events [45].

ACKNOWLEDGMENTS

We acknowledge SOLEIL for provision of synchrotron radiation facilities to E.D., and Dr. Javier Perez for assistance in using the SWING beamline. We thank all the volunteers of GPUGRID who donated GPU computing time to the project. The authors declare that they have no conflict of interest.

FUNDING

This work was supported by Ministero dell'Istruzione, dell'Università e della Ricerca (Grant PRIN 2010-2011), by FISM (Grant 2010), and by Fondazione della Cassa di Risparmio di Teramo TERCAS (Contract 2009-2012) to M.M. G.D.F. acknowledges support by the Spanish Ministry of Science and Innovation (Ref. BIO2011-27450). E.D. and M.M. wish to thank EU for granting the Biostruct-X project within the FP VII programme.

References

1 Simon, G. M. and Cravatt, B. F. (2006) J.Biol.Chem. **281**, 26465-26472

2 Cravatt, B. F., Giang, D. K., Mayfield, S. P., Boger, D. L., Lerner, R. A., and Gilula, N. B. (1996) Nature **384**, 83-87

3 Maccarrone, M. (2006) Curr.Pharm.Des **12**, 759-772

4 Bracey, M. H., Hanson, M. A., Masuda, K. R., Stevens, R. C., and Cravatt, B. F. (2002) Science **298**, 1793-1796

5 Mileni, M., Johnson, D. S., Wang, Z., Everdeen, D. S., Liimatta, M., Pabst, B., Bhattacharya, K., Nugent, R. A., Kamtekar, S., Cravatt, B. F., Ahn, K., and Stevens, R. C. (2008) Proc.Natl.Acad.Sci.U.S.A **105**, 12820-12824

6 Bari, M., Battista, N., Fezza, F., Finazzi-Agro, A., and Maccarrone, M. (2005) J.Biol.Chem. **280**, 12212-12220

7 McFarland, M. J., Porter, A. C., Rakhshan, F. R., Rawat, D. S., Gibbs, R. A., and Barker, E. L. (2004) J.Biol.Chem. **279**, 41991-41997

8 Di Pasquale, E., Chahinian, H., Sanchez, P., and Fantini, J. (2009) PLoS.ONE. **4**, e4989

9 Oddi, S., Dainese, E., Fezza, F., Lanuti, M., Barcaroli, D., De, L., V, Centonze, D., and Maccarrone, M. (2011) J.Neurochem. **116**, 858-865

10 Picazo-Juarez, G., Romero-Suarez, S., Nieto-Posadas, A., Llorente, I., Jara-Oseguera, A., Briggs, M., McIntosh, T. J., Simon, S. A., Ladron-de-Guevara, E., Islas, L. D., and Rosenbaum, T. (2011) J.Biol.Chem. **286**, 24966-24976

11 Kaczocha, M., Lin, Q., Nelson, L. D., McKinney, M. K., Cravatt, B. F., London, E., and Deutsch, D. G. (2012) ACS Chem.Neurosci. **3**, 364-368

12 Maxfield, F. R. and Wustner, D. (2002) J.Clin.Invest **110**, 891-898

13 Forneris, F. and Mattevi, A. (2008) Science **321**, 213-216

14 Fezza, F., Oddi, S., Di Tommaso, M., De Simone, C., Rapino, C., Pasquariello, N., Dainese, E., Finazzi-Agro, A., and Maccarrone, M. (2008) J.Lipid Res. **49**, 1216-1223

15 Guinier, A. and Fournet, G. (1955) Small Angle scattering of X-rays, Wiley, New York

16 Svergun, D. I. (1992) Journal of Applied Crystallography **25**, 495-503

17 Svergun, D. I. and Koch, M. H. (2002) Curr.Opin.Struct.Biol. **12**, 654-660

18 Kozin, M. B. and Svergun, D. I. (2001) Journal of Applied Crystallography **34**, 33-41

19 Dainese, E., Sabatucci, A., van Zadelhoff, G., Angelucci, C. B., Vachette, P., Veldink, G. A., Agro, A. F., and Maccarrone, M. (2005) J.Mol.Biol. **349**, 143-152

20 Volkov, V. V. and Svergun , D. I. (2003) Journal of Applied Crystallography **36**, 860-864

21 Wasilewski, M. and Wojtczak, L. (2005) FEBS Lett. **579**, 4724-4728

22 Dainese, E., Angelucci, C. B., Sabatucci, A., De, F., V, Mei, G., and Maccarrone, M. (2010) FASEB J. **24**, 1725-1736

23 Saslowsky, D. E., Lawrence, J., Ren, X., Brown, D. A., Henderson, R. M., and Edwardson, J. M. (2002) J.Biol.Chem. **277**, 26966-26970

24 Oddi, S., Fezza, F., Pasquariello, N., De Simone, C., Rapino, C., Dainese, E., Finazzi-Agro, A., and Maccarrone, M. (2008) Cell Mol.Life Sci. **65**, 840-850

25 Bolte, S. and Cordelieres, F. P. (2006) J.Microsc. **224**, 213-232

26 Manders, E. M., Stap, J., Brakenhoff, G. J., van, D. R., and Aten, J. A. (1992) J.Cell Sci. **103 (Pt 3)**, 857-862

27 Li, Q., Lau, A., Morris, T. J., Guo, L., Fordyce, C. B., and Stanley, E. F. (2004) J.Neurosci. **24**, 4070-4081

28 Harvey, M. J., Giupponi, G., and Fabritiis, G. D. (2009) J.Chem.Theory Comput. **5**, 1632-1639

29 Buch, I., Harvey, M. J., Giorgino, T., Anderson, D. P., and De, F. G. (2010) J.Chem.Inf.Model. **50**, 397-403

30 MacKerell, A. D., Jr., Feig, M., and Brooks, C. L., III (2004) J.Comput.Chem. **25**, 1400-1415

31 Klauda, J. B., Venable, R. M., Freites, J. A., O'Connor, J. W., Tobias, D. J., Mondragon-Ramirez, C., Vorobyov, I., MacKerell, A. D., Jr., and Pastor, R. W. (2010) J.Phys.Chem.B **114**, 7830-7843

32 Jo, S., Kim, T., Iyer, V. G., and Im, W. (2008) J.Comput.Chem. **29**, 1859-1865

33 Vanommeslaeghe, K., Hatcher, E., Acharya, C., Kundu, S., Zhong, S., Shim, J., Darian, E., Guvench, O., Lopes, P., Vorobyov, I., and MacKerell, A. D., Jr. (2010) J.Comput.Chem. **31**, 671-690

34 Bamber, L., Slotboom, D. J., and Kunji, E. R. (2007) J.Mol.Biol. **371**, 388-395

35 Patricelli, M. P., Lashuel, H. A., Giang, D. K., Kelly, J. W., and Cravatt, B. F. (1998) Biochemistry **37**, 15177-15187

36 Mei, G., Di Venere, A., Gasperi, V., Nicolai, E., Masuda, K. R., Finazzi-Agro, A., Cravatt, B. F., and Maccarrone, M. (2007) J.Biol.Chem. **282**, 3829-3836

37 Nagle, J. F. and Tristram-Nagle, S. (2000) Biochim.Biophys.Acta **1469**, 159-195

38 Dainese, E., Oddi, S., and Maccarrone, M. (2010) Curr.Med.Chem. **17**, 1487-1499

39 Di Venere, A., Dainese, E., Fezza, F., Angelucci, B. C., Rosato, N., Cravatt, B. F., Finazzi-Agro, A., Mei, G., and Maccarrone, M. (2012) Biochim.Biophys.Acta **1821**, 1425-1433

40 Kaczocha, M., Hermann, A., Glaser, S. T., Bojesen, I. N., and Deutsch, D. G. (2006) J.Biol.Chem. **281**, 9066-9075

41 Oddi, S., Fezza, F., Pasquariello, N., D'Agostino, A., Catanzaro, G., De Simone, C., Rapino, C., Finazzi-Agro, A., and Maccarrone, M. (2009) Chem.Biol. **16**, 624-632

42 Buch, I., Giorgino, T., and De, F. G. (2011) Proc.Natl.Acad.Sci.U.S.A **108**, 10184-10189

43 Oradd, G., Lindblom, G., and Westerman, P. W. (2002) Biophys.J. **83**, 2702-2704

44 Hurst, D. P., Grossfield, A., Lynch, D. L., Feller, S., Romo, T. D., Gawrisch, K., Pitman, M. C., and Reggio, P. H. (2010) J.Biol.Chem. **285**, 17954-17964

45 Ortega-Gutierrez, S. (2005) Curr.Drug Targets.CNS.Neurol.Disord. **4**, 697-707

Table 1 Interaction of FAAH with liposomes under different experimental conditions.

LUV membranes	$[L]_{½}$ (μM)
DPPC	65 ± 7
POPC	67 ± 10
POPC:AEA (10:1)	67 ± 8
POPC:ethanolamine (10:1)	100 ± 28
POPC:AA (10:1)	69 ± 10
POPC:cholesterol (10:1)	70 ± 8
POPC:AEA:cholesterol (10:1:1 and 10:1:5)	15 ± 7
Lipid rafts	110 ± 19
Lipid rafts:AEA (10:5)	107 ± 17
Endoplasmic Reticulum	18 ± 3
Plasma Membrane	79 ± 8

Figure Legends

Figure 1 Oligomerisation state of FAAH in solution. Experimental SAXS patterns (A) and pair distribution functions (p(r)) (B) of FAAH in 0.5 M Tris/HCl buffer, pH 7.5. The superposition of the 1MT5 crystal structure with the *ab initio* models of FAAH obtained in solution (C) suggests an oligomer constituted by three octamers.

Figure 2 Effect of detergents that mimic the membrane milieu on FAAH structure. Experimental SAXS pattern of FAAH in the presence of 1% Triton-X100. Inset: Guinier plot including the curve fit (solid line). Arrow: detergent micelle signal.

Figure 3 FAAH activity in the presence of membranes with different lipid compositions. Comparison of the FAAH specific activity normalized to the control measured in solution (100% = 790±30 pmol/min per mg protein), and in the presence of POPC liposomes containing AEA and cholesterol at different molar ratios. ** Denotes $P<0.01$.

Figure 4 Intracellular distribution of FAAH, AEA, and cholesterol in mouse N18 neuroblastoma cells. (a-e) Cells were co-stained for cholesterol (filipin, cyan, a), b-AEA (green, b) and FAAH (red, c). (f-j) Cells were co-stained for b-AEA (cyan, f), FAAH (green, g) and ganglioside GM1 (CTB, red, h). Merged images are shown for the following stainings: filipin with b-AEA (d), filipin with FAAH (e), b-AEA with FAAH (i), and FAAH with CTB (j). The values of the Pearson's correlation coefficient are 0.69 ± 0.03, 0.43 ±0.02, 0.51 ± 0.05, 0.10 ± 0.02, for filipin/b-AEA, filipin/rFAAH, b-AEA/rFAAH, and FAAH/CTB, respectively. Scale bars, 10 μm. Images are representative of three independent experiments, for a total of 18-27 cells. Details are given in the Supplementary Methods, and colocalization values are summarized below.

Figure 5 Molecular dynamics simulations of AEA binding to FAAH. (A) View of the enzyme showing its position in the membrane, the residues of the catalytic triad, an AEA molecule in the membrane, and an ethanolamine molecule exiting. (B) A 2D Histogram shows the position of cholesterol around FAAH in the membrane. The two dark spots show where dimer subunits of FAAH anchor the enzyme to the membrane. Bright spots indicate that cholesterol interacts with the dimer near the entrance ports. (C) Snapshots of cholesterol interaction with the gating residues throughout the binding process. A salt bridge formed by two residues of FAAH (Arg486 and Asp403) is broken before AEA can enter. The hydroxyl head groups of AEA and cholesterol form hydrogen bonds with the residues, allowing them to separate and open the entrance (frame 2). The interaction with cholesterol is maintained throughout the binding process (frames 3,4).

Figure 1

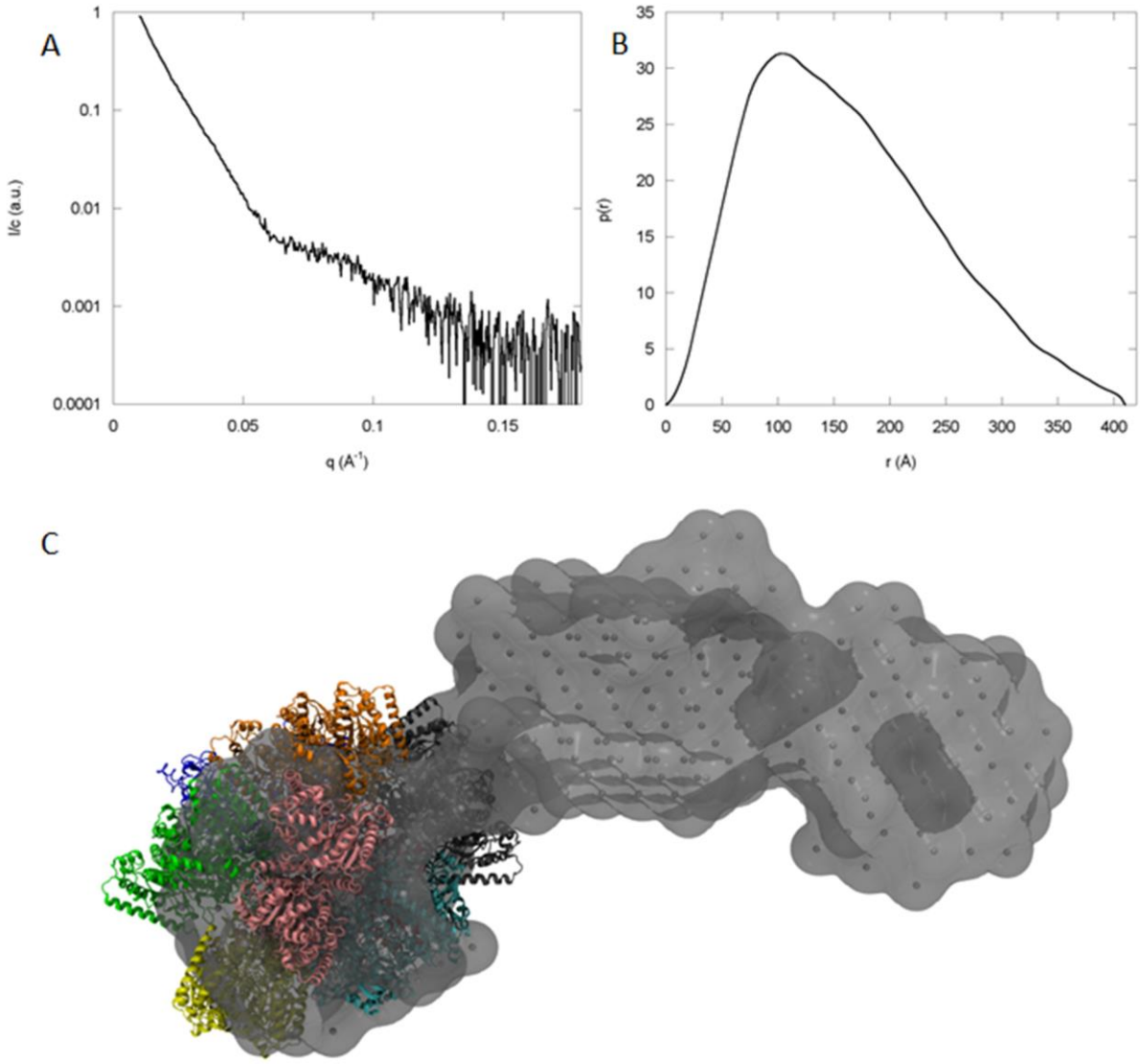
A
B
C
I/c (a.u.)
q (Å^{-1})
p(r)
r (Å)
1
0.1
0.01
0.001
0.0001
0
0.05
0.1
0.15
35
30
25
20
15
10
5
0
50
100
150
200
250
300
350
400

Figure 2

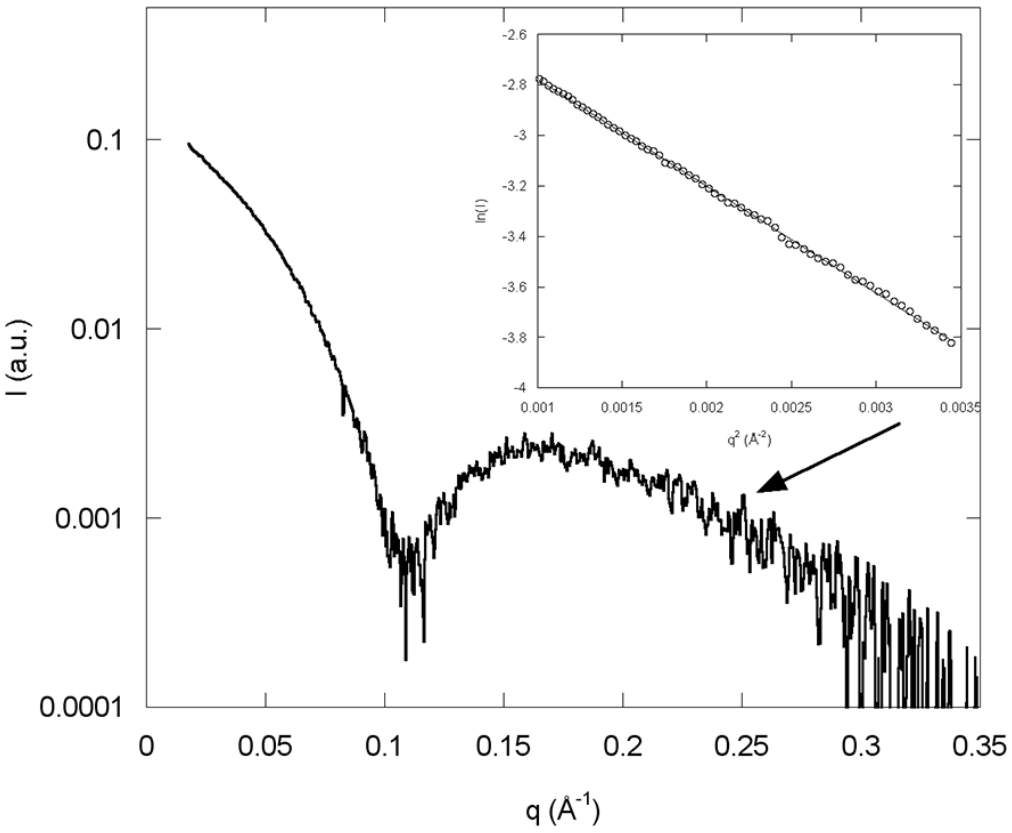
0.1
0.01
0.001
0.0001
I (a.u.)
0
0.05
0.1
0.15
0.2
0.25
0.3
0.35
q (Å^{-1})
-2.6
-2.8
-3
-3.2
-3.4
-3.6
-3.8
-4
ln(I)
0.001
0.0015
0.002
0.0025
0.003
0.0035
q^2 (Å^{-2})

Figure 3

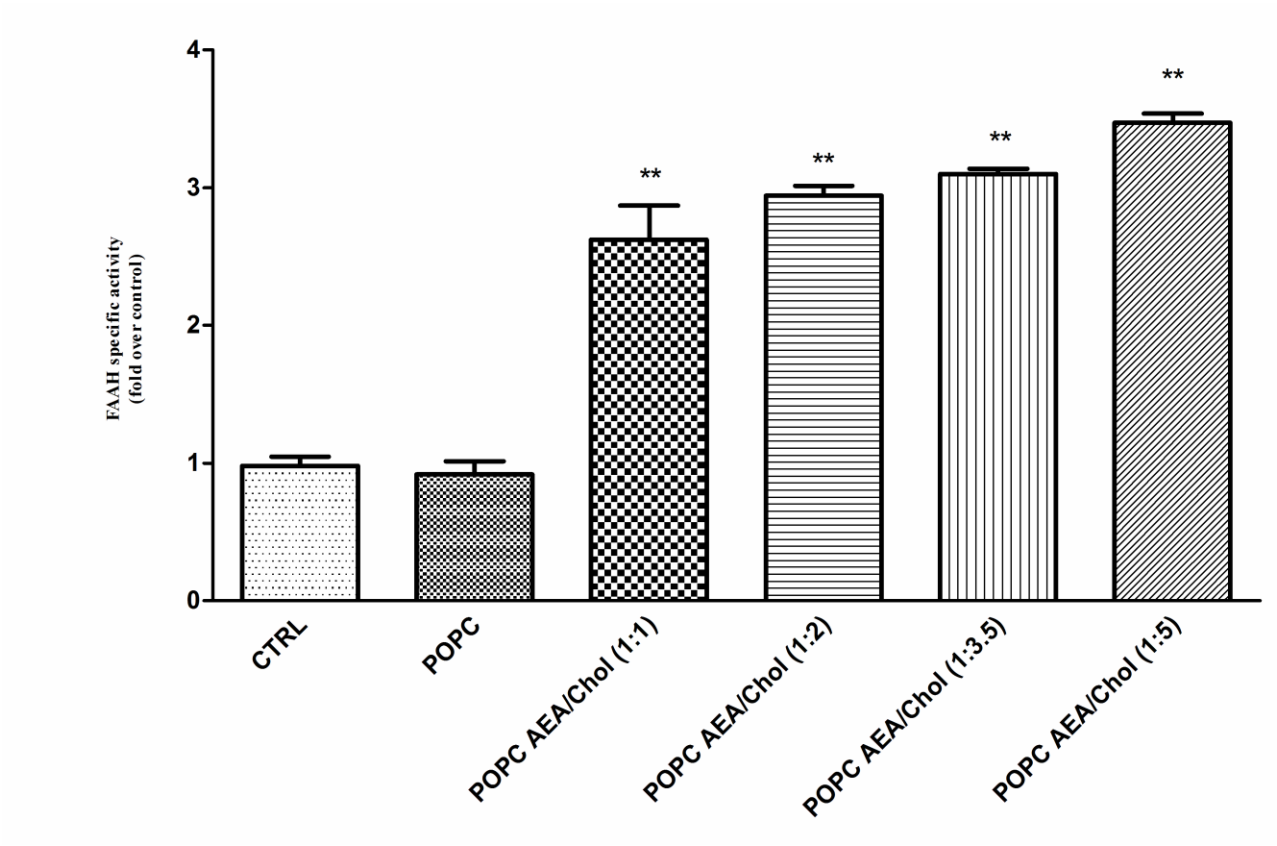
FAAH specific activity
(fold over control)
4
3
2
1
0
**
**
**
**
CTRL
POPC
POPC AEA/Chol (1:1)
POPC AEA/Chol (1:2)
POPC AEA/Chol (1:3.5)
POPC AEA/Chol (1:5)

Figure 4

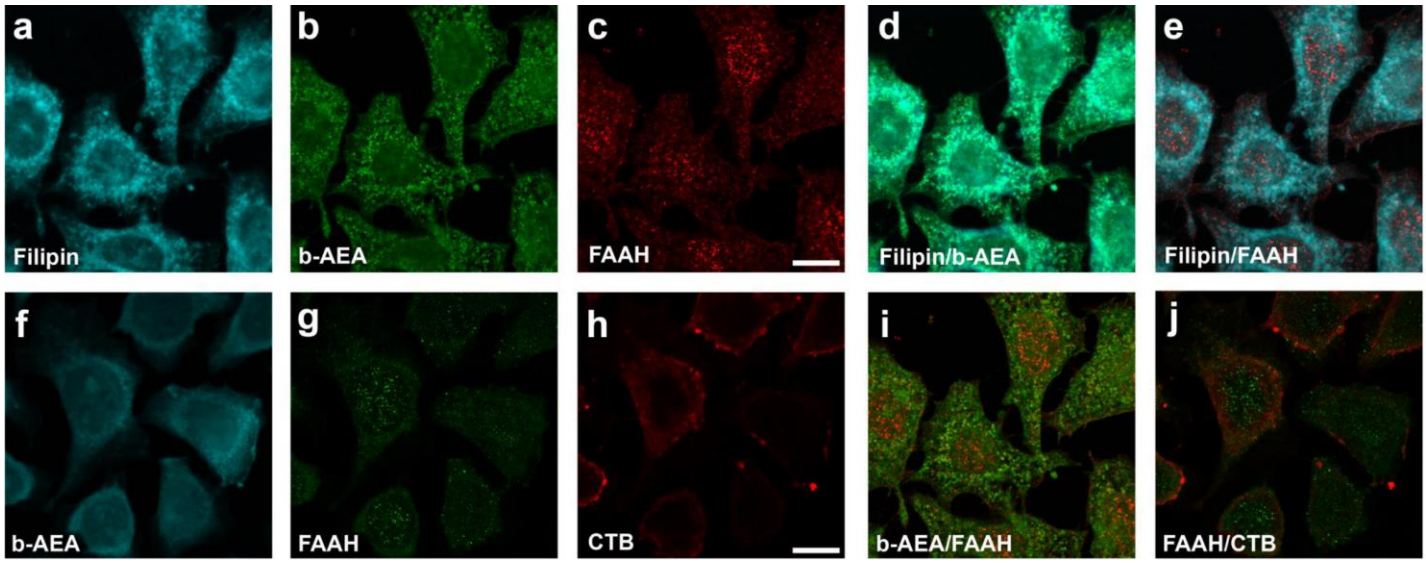
a
Filipin
b
b-AEA
c
FAAH
d
Filipin/b-AEA
e
Filipin/FAAH
f
b-AEA
g
FAAH
h
CTB
i
b-AEA/FAAH
j
FAAH/CTB

Figure 5

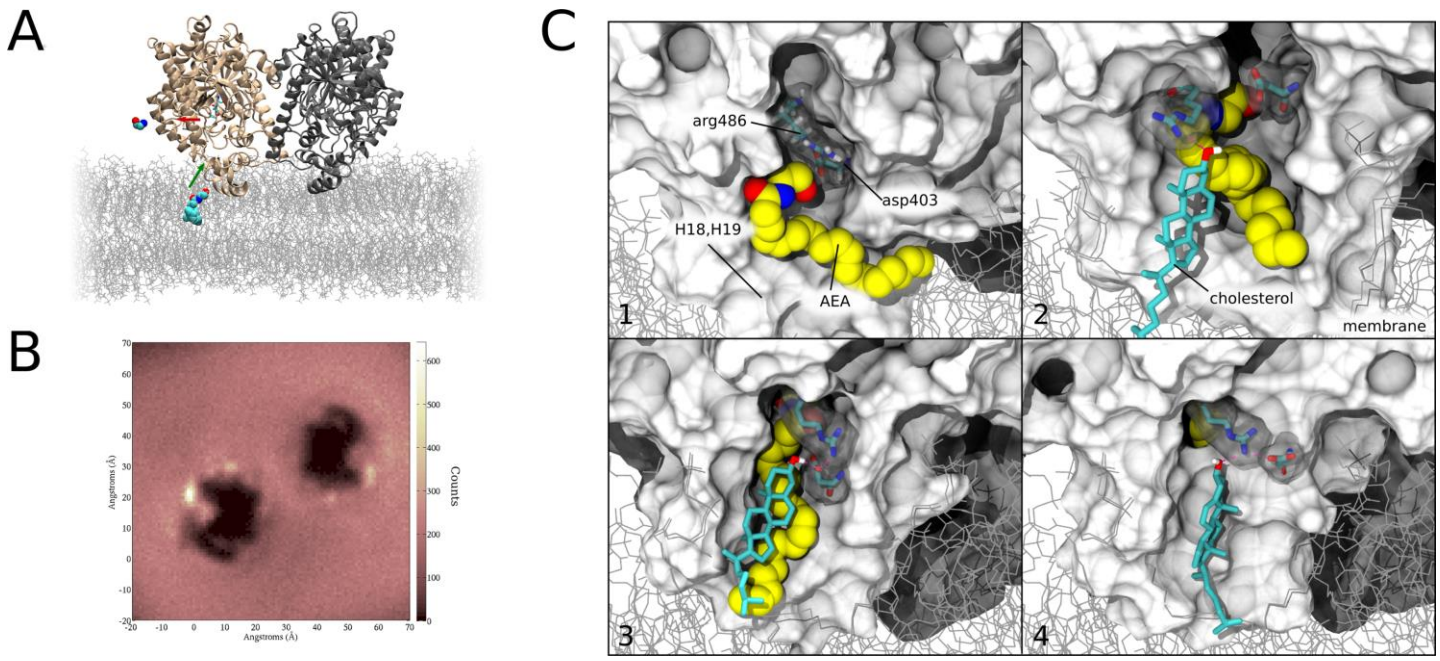
A
B
C
arg486
asp403
H18,H19
AEA
cholesterol
membrane
1
2
3
4
Angstroms (Å)
Angstroms (Å)
Counts